*Articles*

# Complexed Structures of Formylglycinamide Ribonucleotide Amidotransferase from *Thermotoga maritima* Describe a Novel ATP Binding Protein Superfamily†,‡

Mariya Morar,§ Ruchi Anand,§ Aaron A. Hoskins,|| JoAnne Stubbe,⊥ and Steven E. Ealick*,§

*Department of Chemistry and Chemical Biology, Cornell University, Ithaca, New York 14853, and Departments of Chemistry and Biology, Massachusetts Institute of Technology, Cambridge, Massachusetts 02139*

*Received August 5, 2006; Revised Manuscript Received September 12, 2006*

ABSTRACT: Formylglycinamide ribonucleotide amidotransferase (FGAR-AT) catalyzes the ATP-dependent synthesis of formylglycinamidine ribonucleotide (FGAM) from formylglycinamide ribonucleotide (FGAR) and glutamine in the fourth step of the purine biosynthetic pathway. FGAR-AT is encoded by the *purL* gene. Two types of PurL have been detected. The first type, found in eukaryotes and Gram-negative bacteria, consists of a single 140 kDa polypeptide chain and is designated large PurL (lgPurL). The second type, small PurL (smPurL), is found in archaea and Gram-positive bacteria and consists of an 80 kDa polypeptide chain. SmPurL requires two additional gene products, PurQ and PurS, for activity. PurL is a member of a protein superfamily that contains a novel ATP-binding domain. Structures of several members of this superfamily are available in the unliganded form. We determined five different structures of FGAR-AT from *Thermotoga maritima* in the presence of substrates, a substrate analogue, and a product. These complexes have allowed a detailed description of the novel ATP-binding motif. The availability of a ternary complex enabled mapping of the active site, thus identifying potential residues involved in catalysis. The complexes show a conformational change in the active site compared to the unliganded structure. Surprising discoveries, an ATP molecule in an auxiliary site of the protein and the conformational changes associated with its binding, provoke speculation about the regulatory role of the auxiliary site in formation of the PurLSQ complex as well as the evolutionary relationship of PurLs from different organisms.

The purine biosynthetic pathway is ubiquitous in most living organisms, and it is a 10-step process for converting phosphoribosyl pyrophosphate to inosine monophosphate. Formyl glycinamide ribonucleotide amidotransferase (FGAR-AT),[1] also known by its gene product name, PurL, catalyzes the fourth step in the pathway, conversion of formylglycinamide ribonucleotide (FGAR) to formylglycinamidine ribonucleotide (FGAM) (Scheme 1) (*1*). In this reaction, glutamine is converted to glutamate, releasing ammonia, which is incorporated into the amide of FGAR and ATP is converted to ADP and $P_i$.

Scheme 1

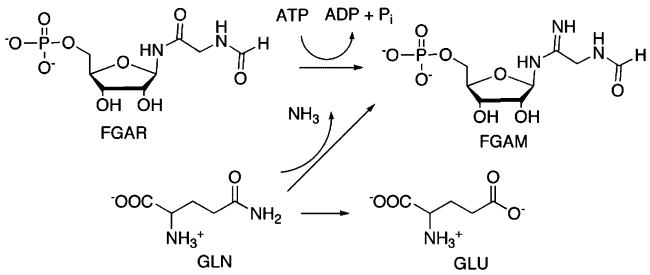


ATP-utilizing proteins are grouped into superfamilies on the basis of their unique ATP-binding motif. Among these protein superfamilies are the classical dinucleotide motif, the classical mononucleotide motif, the kinase motif, and the ATP grasp motif (*2*−*4*). Of the five ATP-utilizing enzymes

† This work was supported by the NIH Grants RR15301 and GM073220 (S.E.E.). S.E.E. is indebted to the W. M. Keck Foundation and the Lucille P. Markey Charitable Trust. A.A.H. was supported by a NSF predoctoral fellowship. A.A.H. and J.S. were supported by NIH Grant GM32191. The Biophysical Instrumentation Facility for the Study of Complex Macromolecular Systems at the Massachusetts Institute of Technology is supported by NSF Grant 0070319 and NIH Grant GM68762.

‡ The coordinates of the TmPurL structures have been deposited in the Protein Data Bank as entries 2HRU for the PurL−ADP complex, 2HRY for the PurL−AMPPCP complex, 2HS0 for the PurL−ATP/ATP complex, 2HS3 for the PurL−FGAR complex, and 2HS4 for the PurL−FGAR−AMPPCP complex.

* To whom correspondence should be addressed: Department of Chemistry and Chemical Biology, Cornell University, Ithaca, NY 14853. Telephone: (607) 255-7961. Fax: (607) 255-1227. E-mail: see3@cornell.edu.

§ Cornell University.

|| Department of Chemistry, Massachusetts Institute of Technology.

⊥ Department of Biology, Massachusetts Institute of Technology.

[1] Abbreviations: FGAR-AT, formylglycinamide ribonucleotide amidotransferase; FGAM, formylglycinamidine ribonucleotide; FGAR, formylglycinamide ribonucleotide; PRPP, phosphoribosyl pyrophosphate; IMP, inosine 5′-monophosphate; AIR, aminoimidazole ribonucleotide; GAR, glycinamide ribonucleotide; AMPPCP, $\beta,\gamma$-methylene adenosine 5′-triphosphate; PEP, phosphoenolpyruvate; NADH, nicotinamide adenine dinucleotide hydride; HEPES, 4-(2-hydroxyethyl)-1-piperazineethanesulfonic acid; PK, pyruvate kinase; LDH, lactate dehydrogenase; Tm, *Thermotoga maritima*; St, *Salmonella typhimurium*; Aa, *Aquifex aeolicus*; Ec, *Escherichia coli*; wt, wild type; rmsd, root-mean-square deviation; U, unit of enzyme activity (micromoles of product per minute); lgPurL, large PurL; smPurL, small PurL; asu, asymmetric unit.

10.1021/bi061591u CCC: $33.50 
Published on Web 11/22/2006

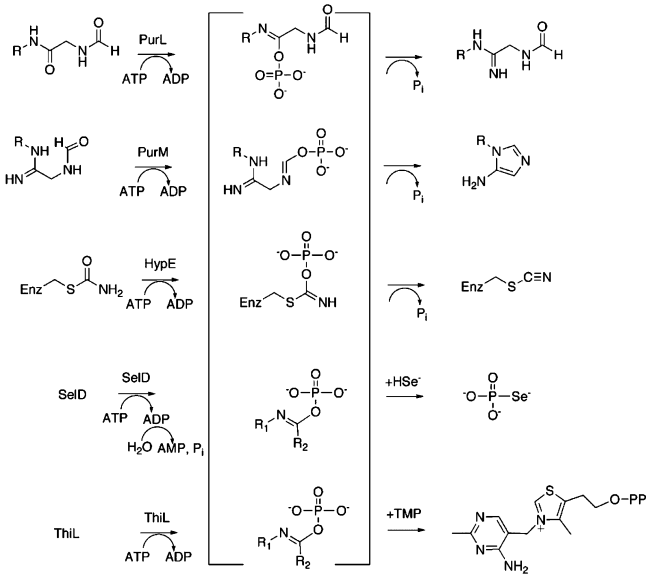


FIGURE 1: Overview of the reactions catalyzed by the members of the PurM superfamily. R is ribose 5′-phosphate. $R_1$ is H or protein backbone. $R_2$ is the Asn/Gln side chain or protein backbone. TMP stands for thiamine monophosphate. Proposed intermediates are shown in brackets.

in the purine biosynthetic pathway of prokaryotes, three belong to the ATP grasp superfamily and two, PurL and aminoimidazole ribonucleotide (AIR) synthetase (PurM), are members of the recently discovered PurM superfamily (*5*). The PurM superfamily contains a poorly characterized ATP-binding motif, which was identified through multiple-sequence alignments with a signature sequence, $DX_4GAXP$, present in all of the family members (*6*). To date, five enzymes are considered to be part of this superfamily: PurM, PurL, selenophosphate synthetase (SelD), iron−nickel hydrogenase maturation protein (HypE), and thiamine phosphate kinase (ThiL) (*6*).

Besides the signature sequence, the PurM superfamily members are thought to be united by a similar catalytic mechanism (Figure 1). PurM catalyzes the conversion of FGAM to AIR in the fifth step of the purine biosynthetic pathway. This reaction is remarkably similar to that catalyzed by PurL, and both may act through an iminophosphate intermediate (*6*). This intermediate, also proposed for HypE, has become another hallmark of the PurM superfamily (*7*). Little is known about this aspect of the mechanism of SelD and ThiL; however, a phosphorylated enzyme intermediate is a possibility.

PurLs from eukaryotic (chicken and pigeon livers), Gram-negative (*Escherichia coli*), and Gram-positive bacteria (*Bacillus subtilis*) have been investigated in an effort to elucidate their reaction mechanism(s) (*8*, *9*). These studies revealed that PurL exists in two forms, designated large PurL (lgPurL) and small PurL (smPurL). LgPurL is approximately 140 kDa and has been found in eukaryotes and Gram-negative organisms. Structure and sequence alignments reveal that it consists of three major domains: the FGAM synthetase domain, the glutaminase domain responsible for the hydrolysis of glutamine and generation of ammonia, and the N-terminal domain which may be involved in formation of the ammonia channel (*10*). Surprisingly, a tightly bound $(Mg^{2+})_3$-ADP species was found in the crystal structure of StPurL in an auxiliary nucleotide binding site, which is related by symmetry to the active site. SmPurL, with a molecular mass between 66 and 80 kDa, is found in archaea and Gram-positive bacteria. This enzyme is homologous to the FGAM synthetase domain of lgPurL and requires two other gene products, PurQ and PurS, for activity. PurQ is equivalent to the glutaminase domain, and a PurS dimer is structurally homologous to the N-terminal domain of lgPurL (*11*, *12*). Recently, the PurLSQ complex from *B. subtilis* was reconstituted and its formation shown to be dependent on the presence of small molecules: MgADP and glutamine (*13*). The formation of the complex, its stability, and the channeling of ammonia between proteins of the complex are not yet well-understood processes.

The phosphorylated FGAR intermediate also remains elusive, although the Stubbe laboratory showed using $^{18}O$ labeling experiments that the amide carbonyl oxygen of FGAR is transferred to inorganic phosphate (*9*). Four structures of various unliganded members of the PurM superfamily are now available [*E. coli* PurM (PDB entry 1CLI), *Salmonella typhimurium* PurL (PDB entry 1T3T), *Thermotoga maritima* PurL (PDB entry 1VK3), and *Aquifex aeolicus* ThiL (PDB entry 1VQV)], but none contain a detailed description of the ATP binding pocket due to the lack of a nucleotide complex. To characterize the ATP and FGAR binding sites, and to obtain more information about the key features of the reaction, we undertook a crystallographic study of smPurL from *T. maritima* complexed with various substrates, products, and substrate analogues. Mutagenesis and biochemical assays confirmed the identification of two residues that are important for catalysis.

## EXPERIMENTAL PROCEDURES

*Materials and Methods.* $\beta$-FGAR was prepared from chemically synthesized $\alpha/\beta$-GAR using glycinamide ribotide transformylase (PurT) as previously described (*14*). The PurT plasmid was a gift from H. Holden (University of Wisconsin, Madison, WI) (*15*). *E. coli* PurM containing an N-terminal histidine tag was purified as described previously (His-PurM, specific activity of 1−2 units/mg) (*6*). ATP, ADP, phosphoenolpyruvate, NADH, and pyruvate kinase (PK)/lactate dehydrogenase (LDH) (a premixed glycerol solution with 660 units/mL PK and 1350 units/mL LDH) were purchased from Sigma. $NH_4Cl$ was from Mallinckrodt. All spectrophotometric assays were carried out on a Cary 3 UV−vis spectrophotometer with temperature regulation using a Lauda water bath. Circular dichroism and analytical ultracentrifugation experiments were carried out in the Biophysical Instrumentation Facility for the Study of Complex Macromolecular Systems [Department of Chemistry, Massachusetts Institute of Technology (MIT)].

*Cloning of TmPurL*. The *T. maritima purL* gene was cloned from genomic DNA (ATCC) by standard PCR procedures using the KOD HiFi DNA polymerase (Novagen) and the primers TML-NdeI and TML-NotI (primers 1 and 2, Table 1 of the Supporting Information). Taq DNA polymerase (Invitrogen) was then used to create 3′-A overhangs on the PCR product, which was subsequently ligated into the pCRII-TOPO vector (Invitrogen) in a topoisomerase-dependent reaction to make pCRII-TOPO-TML. Colonies containing the insert were selected by blue-white screening on X-Gal-containing media. The insert was

isolated from the pCRII-TOPO-TML plasmid by digestion with NdeI and NotI (New England BioLabs) and ligated into pET-24a (Novagen) at the same restriction sites to create pET-TML. Sequencing of the gene by the MIT Biopolymers Facility revealed a silent mutation at nucleotide position 891 corresponding to an ATC → ATT change in the Ile codon.

*Mutagenesis of TmPurL*. H72A and H32A TmPurL mutants were prepared using standard site-directed mutagenesis procedures with primers 3 and 5 (Table 1 of the Supporting Information) (*16*, *17*). The H32Q and H72Q mutants were prepared using a Quikchange mutagenesis kit (Stratagene) following standard procedures and primers 4 and 6 (Table 1 of the Supporting Information).

*Expression and Purification of wt and Mutant TmPurLs*. The pET-TML plasmid containing either the wild type (wt) or the mutant PurL gene was transformed into Rosetta(DE3) *E. coli* (Novagen). Single colonies were used to inoculate 5 mL of LB medium supplemented with 35 $\mu$g/mL kanamycin and 30 $\mu$g/mL chloramphenicol and grown overnight at 37 °C. The saturated culture was then used to inoculate 1 L of LB medium containing the same antibiotics. The cell culture was grown at 37 °C with shaking at 200 rpm, and after an $OD_{600}$ of 0.7 was reached, the cells were induced with 200 $\mu$M isopropyl $\beta$-D-thiogalactopyranoside at 25 °C for 6 h. The cell pellet, usually ~4 g/L, was collected by centrifugation and stored at −80 °C.

Cells (~4 g) were resuspended in 40 mL of TM buffer [50 mM HEPES (pH 7.8) and 100 mM NaCl] with the addition of COMPLETE Protease Inhibitors (Roche) and lysed by sonication while being cooled in an ice/water bath. A Sonic Dismembrator 550 device from Fischer Scientific was used with a $^1/_4$ in. thick flat tip and a 5 s pulse followed by cooling for 5 s over a period of 6 min. Cell debris was removed by centrifugation at 17 000 rpm for 20 min. The lysate was then loaded onto a HiTrap MonoQ FF column (10/10, Pharmacia) equilibrated in TM buffer and washed until the $A_{280}$ was <0.1. The protein was eluted with a 0.1 to 1 M NaCl gradient (150 × 150 mL) at a flow rate of 2 mL/min while collecting 5 mL fractions. Fractions containing TmPurL eluted at ~200 mM NaCl and were concentrated to 10 mL using a YM30 Centricon (Millipore).

The concentrated protein was desalted with a Hi-Load Superdex 75 column (26/60, Pharamacia) equilibrated in TM buffer. Protein was eluted with TM buffer at a flow rate of 2 mL/min, and 2 mL fractions were collected. Protein-containing fractions were concentrated to 10 mg/mL and frozen in liquid $N_2$. Typical protein yields were ~20 mg of protein/g of cells. All of the TmPurL mutants (H32A, H32Q, H72A, and H72Q) were expressed and purified following the same protocol that was used for the wt protein (Figure 1 of the Supporting Information).

*Crystallization of TmPurL*. Initial crystallization conditions were determined using Hampton Research Crystal Screen 1 and Crystal Screen 2. The hanging drop method was used; the drops contained 2 $\mu$L of protein and 2 $\mu$L of well solution. The protein concentration was 10 mg/mL in 25 mM HEPES (pH 7.7) and 50 mM NaCl. The optimized crystallization condition was as follows: 17% PEG 4K, 4% 2-propanol, and 100 mM HEPES (pH 7.3). The crystals grew in 1−2 days. The crystals of the TmPurL−ATP complex were obtained by soaking the sample with 1 mM ATP and 2 mM $MgCl_2$ in mother liquor for 30 min. The TmPurL−FGAR complex was obtained by cocrystallization of 1 mM FGAR and TmPurL using the same conditions that were used for native TmPurL. For the ternary complex, the TmPurL−FGAR cocrystals were soaked with 1 mM AMPPCP, 1 mM $MgCl_2$, and 2 mM FGAR in mother liquor for 1 h. The H72A mutant was crystallized in 17% PEG 4K, 8% 2-propanol, and 100 mM HEPES (pH 7.1). The H72A TmPurL−AMPPCP complex was obtained by soaking the sample in mother liquor with addition of 1 mM FGAR, 1 mM $MgCl_2$, and 1 mM AMPPCP for 2 h. The crystals for the H72A TmPurL−ADP complex were obtained by soaking the sample with 1 mM FGAR, 1 mM $MgCl_2$, and 1 mM ADP. All of the crystals were frozen in liquid nitrogen with 12% glycerol with mother liquor serving as the cryoprotectant.

*Data Collection and Processing*. The data sets for the TmPurL−ATP/ATP, TmPurL−FGAR, and TmPurL−FGAR−AMPPCP complexes were collected at the 8-BM beam line of the Advanced Photon Source (APS) at Argonne National Laboratory (Argonne, IL). A Quantum 315 detector was used for data collection with oscillation steps of 0.5°, an exposure time of 40 s, and a crystal−detector distance of 300 mm for all of the data sets. The data set for the H72A−TmPurL complex with AMPPCP was collected at the SER-CAT beam line of APS. A MAR 300 detector was used to record X-ray intensities. The data were collected at 1° oscillation with 5 s exposures for a total of 100° and a crystal−detector distance of 200 mm. The data for the H72A TmPurL−ADP complex were collected at the 8-BM beam line of APS. The data were collected using a Quantum 315 detector at 0.5° oscillation with 30 s exposures and a crystal−detector distance of 300 mm.

The HKL2000 program suite was used to integrate and scale all data sets (*18*). The TmPurL−FGAR cocrystal data set was processed in monoclinic space group $P2_1$ with the following unit cell dimensions: $a = 69.7$ Å, $b = 57.4$ Å, $c = 75.5$ Å, and $\beta = 114.2°$. The asymmetric unit (asu) contains one monomer; the calculated solvent content is 43%. The data for the TmPurL−FGAR−AMPPCP complex were in orthorhombic space group $P2_12_12_1$ with one monomer per asu, 45% solvent content, and the following cell dimensions: $a = 58.4$ Å, $b = 71.5$ Å, and $c = 138.3$ Å. The TmPurL−ATP/ATP complex data were processed in space group $P2_12_12_1$ with one monomer per asu, 43% solvent, and the following cell dimensions: $a = 56.9$ Å, $b = 71.5$ Å, and $c = 137.4$ Å. The H72A TmPurL−AMPPCP complex was in orthorhombic space group $P2_12_12_1$ with the following cell dimensions: $a = 56.6$ Å, $b = 70.0$ Å, and $c = 133.5$ Å. The asu contains one monomer, and the calculated solvent content is 41%. The H72A TmPurL−ADP complex was in the $P2_12_12_1$ space group with one monomer per asu, 43% solvent content, and the following cell dimensions: $a = 56.6$ Å, $b = 71.0$ Å, and $c = 137.0$ Å. Final data processing statistics are listed in Table 1.

*Structure Determination and Refinement*. Phases for both wt and mutant TmPurL complexes were obtained by molecular replacement using the deposited TmPurL structure (PDB entry 1VK3). Rotation and translation were performed using the CNS program suite with the data cutoff being at 4.0 Å resolution (*19*). CNS and CCP4 programs were used to refine all the structures (*20*). Several rounds of minimization, simulated annealing, temperature factor refinement in

Table 1: Summary of Data Collection and Processing Statistics[a]

| | TmPurL−FGAR | H72A TmPurL−AMPPCP | H72A TmPurL−ADP | TmPurL−FGAR−AMPPCP | TmPurL−ATP/ATP |
|---|---|---|---|---|---|
| resolution (Å) | 2.3 | 2.8 | 2.8 | 2.7 | 2.5 |
| wavelength (Å) | 0.979 | 0.999 | 0.979 | 0.979 | 0.979 |
| space group | $P2_1$ | $P2_12_12_1$ | $P2_12_12_1$ | $P2_12_12_1$ | $P2_12_12_1$ |
| no. of reflections | 39507 | 48531 | 56163 | 71415 | 74573 |
| no. of unique reflections | 19579 | 13589 | 14120 | 15867 | 18839 |
| redundancy | 2.2 (2.1) | 3.6 (3.7) | 4.0 (4.0) | 4.6 (4.4) | 4.0 (3.9) |
| completeness | 79.4 (78.4) | 98.3 (98.9) | 90.5 (96.7) | 97.7 (98.1) | 96.2 (96.0) |
| $R_{sym}$ (%)[b] | 9.1 (22.4) | 10.9 (38.9) | 8.2 (36.8) | 14.0 (38.8) | 10.7 (28.7) |
| $I/\sigma$ | 9.2 (3.2) | 9.6 (2.9) | 16.8 (3.5) | 8.8 (3.6) | 9.8 (4.7) |

[a] Values for the highest-resolution shell are given in parentheses. [b] $R_{sym} = \sum\sum_i|I_i - \langle I\rangle|/\sum\langle I\rangle$, where $\langle I\rangle$ is the mean intensity of $N$ reflections with intensities $I_i$ and common indices $h$, $k$, and $l$.

Table 2: Refinement Statistics

| | TmPurL−FGAR | H72A TmPurL−AMPPCP | H72A TmPurL−ADP | TmPurL−FGAR−AMPPCP | TmPurL−ATP/ATP |
|---|---|---|---|---|---|
| resolution (Å) | 50−2.3 | 20−2.8 | 50−2.8 | 43−2.7 | 32−2.5 |
| total no. of non-hydrogen atoms | 5113 | 4703 | 4626 | 4852 | 4755 |
| no. of proteins | 4618 | 4429 | 4476 | 4625 | 4473 |
| no. of ligands | 24 | 38 | 30 | 63 | 78 |
| no. of waters | 471 | 236 | 120 | 164 | 204 |
| no. of reflections in refinement | 17841 | 12154 | 11559 | 15163 | 18234 |
| no. of reflections in test set | 900 | 653 | 616 | 741 | 896 |
| $R$ factor (%)[a] | 19.3 | 18.5 | 20.8 | 19.1 | 20.0 |
| $R_{free}$ (%)[b] | 25.0 | 28.3 | 27.6 | 26.6 | 25.3 |
| rms deviation from ideal geometry | | | | | |
| bonds (Å) | 0.006 | 0.007 | 0.007 | 0.006 | 0.007 |
| angles (deg) | 1.4 | 1.4 | 1.4 | 1.4 | 1.4 |
| average $B$ factor (Å$^2$) | 23.7 | 26.0 | 42.0 | 24.1 | 24.7 |
| Ramachandran plot | | | | | |
| most favored region (%) | 87.7 | 84.4 | 83.2 | 86.0 | 89.8 |
| additional allowed region (%) | 11.5 | 15.2 | 15.4 | 12.8 | 9.6 |
| generously allowed region (%) | 0.6 | 0.2 | 1.2 | 1.0 | 0.4 |
| disallowed region (%) | 0.2 | 0.2 | 0.2 | 0.2 | 0.2 |

[a] $R$ factor $= \sum_{hkl}||F_{obs}| - k|F_{cal}||/\sum_{hkl}|F_{obs}|$, where $F_{obs}$ and $F_{cal}$ are observed and calculated structure factors, respectively. [b] $R_{free}$ is the sum extended over a subset of reflections that were excluded from all stages of refinement.

CNS, and Refmac5 refinement in CCP4i followed by manual map refitting in O (*21*) were performed. A composite omit map was used when the models were refined manually. Water molecules were included in subsequent rounds of refinement on the basis of the criteria that the peak in difference electron density maps was higher than $2\sigma$ and the water molecule formed at least one hydrogen bond with a protein, ligand, or solvent atom. Final data refinement statistics are listed in Table 2.

*Protein Concentration Determination.* Protein concentrations were calculated using the $\epsilon_{280}$ [51 610 $M^{-1}$ $cm^{-1}$ obtained from ProtParam from the EXPASY website (www.expasy.ch)].

*Sedimentation Velocity Analytical Ultracentrifugation (SV-AUC).* SV-AUC experiments were performed using an Optima XL-1 analytical ultracentrifuge (Beckman Coulter, Fullerton, CA). Before each experiment, protein samples were dialyzed against 50 mM Tris (pH 8.0), 20 mM KCl, and 20 mM $MgCl_2$ for 24 h in a Slide-A-Lyzer cassette with a 10 kDa molecular mass cutoff (MWCO) membrane (Pierce). Samples (400 $\mu$L) were then diluted to 9.7 $\mu$M and placed in double-sector Epon centerpieces with quartz windows in an An60Ti four-hole rotor. Sedimentation was monitored at 30 000 rpm for 24 h at 25 °C by continuous scanning at 280 nm along the length of the cell.

SEDNTERP software from J. Philo was used to calculate buffer density (1.00197 g/mL), viscosity (0.01002 P), and protein partial specific volume from the amino acid content (0.7444 mL/g) (*22*). Data (~100 traces for each experiment) were fit using SEDFIT88 from 0.5 to 20 S using a continuous distribution of sedimentation coefficients derived from solutions to Lamm equations (*23*).

*Circular Dichroism Spectroscopy.* Circular dichroism (CD) spectra were collected on an AVIV model 202 CD spectrophotometer (AVIV Biomedical, Inc., Lakewood, NJ). Proteins were dialyzed before the experiment against 10 mM $K_2HPO_4$ buffer (pH 7.0) for 16 h using a Slide-A-Lyzer cassette (Pierce) with a 10 kDa MWCO membrane. Spectra were collected for each sample (5 $\mu$M) at 25 °C in a 0.1 cm path length quartz cuvette in argon-degassed dialysis buffer

by scanning from 300 to 190 nm at 0.5 nm increments with a 0.2 s integration time.

*Quantitation of Binding of [8-$^{14}$C]ADP or [8-$^{14}$C]ATP to TmPurL.* TmPurL (45 nmol) was added to a final volume of 250 $\mu$L containing 50 mM Tris (pH 8.0), 20 mM KCl, 20 mM $MgCl_2$, and either 3 mM [8-$^{14}$C]ADP (658 cpm/nmol, Moravek Biochemicals, Brea, CA) or 3 mM [8-$^{14}$C]ATP (659 cpm/nmol, MP Biomedical, Irvine, CA), and the reaction mixture was incubated at 37 °C for 5 min. The [8-$^{14}$C]ATP-containing solutions also contained 1.5 mM PEP and 4 units/mL PK (451 units/mg Sigma P-7768).

After being incubated, the sample was then applied directly to a Sephadex G-50 column (1 cm × 20 cm, Sigma) equilibrated with 50 mM Tris (pH 8.0), 20 mM KCl, and 20 mM $MgCl_2$ at room temperature. Fractions of 0.5 mL were collected, and 0.2 mL was mixed with 7 mL of Emulsifier-Safe scintillation fluid (Perkin-Elmer) and analyzed by scintillation counting. The remainder of the fraction was characterized by UV absorbance at 260 and 280 nm using a Bio-Rad Ultramark plate reader in a 96-well UV-transparent plate (Corning). Protein content was quantified using a Lowry assay (*24*) against a BSA standard and by the $A_{280}$.

*Enzyme Assays*. TmPurL was assayed in the absence of PurS and PurQ by monitoring $NH_4Cl$-dependent FGAM formation. FGAM synthesis was monitored directly using a coupled, discontinuous assay with His-PurM and the modified Bratton−Marshall assay (*9*). Each assay contained, in a final volume of 400 $\mu$L, 100 mM Tris (pH 8.0), 20 mM KCl, 20 mM $MgCl_2$, 1.5 mM PEP, 10 units/mL PK, 20 units/mL His-PurM, 750 mM $NH_4Cl$, 10 mM ATP, and 5 mM $\beta$-FGAR. The reaction was initiated by the addition of enzyme (∼1−10 $\mu$g) and the mixture incubated at 37 °C before the reaction was quenched with 100 $\mu$L of 1.33 M $K_2HPO_4$ (pH 1.4) and 20% trichloroacetic acid followed by derivitization and quantitation of AIR (*9*).

ADP formation was assessed using a coupled assay at 37 °C with PK and LDH, monitoring NADH oxidation at 340 nm ($\epsilon$ = 6200 $M^{-1}$ $cm^{-1}$). The assay buffer was the same as described above except that it also contained 0.2 mM NADH, 20 units/mL PK, and 42 units/mL LDH.

*Determination of Kinetic Constants*. Kinetic parameters for ATP were determined using the PK/LDH coupled assay with 0−10 mM ATP in the presence of saturating amounts of FGAR (5 mM) and $NH_4Cl$ (750 mM). Kinetic parameters for FGAR were determined using the Bratton−Marshall assay with 0−5 mM FGAR in the presence of saturating amounts of ATP (10 mM) and $NH_4Cl$ (750 mM). For H72A TmPurL, the concentration of FGAR was varied from 0 to 32 mM. Parameters for $NH_4Cl$ were determined using the Bratton−Marshall assay with 0−750 mM $NH_4Cl$ in the presence of saturating amounts of ATP (10 mM) and FGAR (5 mM). Data were analyzed using a nonlinear regression analysis with KaleidaGraph (Synergy) and eq 1.

$$v = V_{max}[S]/(K_m + [S]) \quad (1)$$

*Preparation of Figures.* All figures were prepared using ChemDraw, MOLSCRIPT (*25*), and PYMOL (*26*). All the stereoview figures were prepared using PYMOL and RASTER3D (*27*).

## RESULTS

*Structure Determination and Quality Assessment for the Final Models*. The three-dimensional structures of the TmPurL complexes were determined by molecular replacement using the deposited TmPurL structure determined by the Joint Center for Structural Genomics (JCSG, PDB entry 1VK3) as the search model (*19*). The resolution for the structures ranged from 2.3 to 2.8 Å, and the results, including final $R$ factors and $R_{free}$ values, are summarized in Table 2.

TmPurL consists of 603 residues with a molecular mass of 66 kDa; however, all five structures have disordered regions. In the TmPurL−ATP/ATP complex, and both H72A TmPurL−AMPPCP and H72A TmPurL−ADP complex structures, residues 186−207 were excluded from the model due to the lack of clear density. This region was also missing in the deposited structure. In the TmPurL−FGAR and TmPurL−FGAR−AMPPCP complexes, residues 186−207 are ordered and present in the final models. Due to poor electron density, residues 48−55 are absent from the H72A TmPurL−AMPPCP structure, and residues 373−378 are absent from the TmPurL−ATP/ATP structure. All structures contained one residue, Leu551, in the disallowed region of the Ramachandran plot. This residue is located in a tight turn involved in the binding of the phosphate tail of the auxiliary ATP, and its electron density is unambiguous. The quality of all models was verified using PROCHECK (*28*).

*Overall Structure.* The fold of TmPurL is very similar to that of the FGAM synthetase domain of large *S. typhimurium* PurL (StPurL) (*10*). As in the FGAM synthetase domain of StPurL, TmPurL can be divided into four subdomains: A1 and A2 make up the core of the enzyme, B1 is the N-terminal subdomain, and B2 is the C-terminal subdomain (Figure 2A and Figure 2 of the Supporting Information). The core of the enzyme contains a central mixed $\beta$-barrel made of eight long strands from subdomains A1 ($\beta$1−$\beta$4) and A2 ($\beta$13−$\beta$16). The barrel is flanked by four helices: α5 and α6 on the N-terminal side (A1 subdomain) and α14 and α15 on the C-terminal side (A2 subdomain). The B1 subdomain consists of a seven-stranded mixed sheet, three long helices (more than 10 residues in length), and three short helices. The helices form most of the interdomain contacts with the A1 subdomain, while the sheet is more solvent-exposed. The B2 subdomain is the smallest of the four. It contains a five-stranded antiparallel $\beta$-sheet which is flanked by two helices. The helices come in contact with the A2 subdomain, while the sheet is exposed to the solvent.

*Nucleotide Binding in the Active Site.* Four structures of TmPurL complexed with various nucleotides were obtained. A ternary complex of TmPurL with a nonhydrolyzable ATP analogue, $(Mg^{2+})_2$-AMPPCP, and FGAR was obtained from cocrystallization of the enzyme with FGAR and soaking with AMPPCP and $MgCl_2$. Soaking of the wt enzyme with $MgCl_2$ and ATP yielded a structure with $(Mg^{2+})$-ATP in the active and auxiliary sites, resulting in the TmPurL−ATP/ATP structure. Soaking of the H72A mutant TmPurL crystal with FGAR, AMPPCP, and $MgCl_2$ yielded a structure with $(Mg^{2+})_2$-AMPPCP in the active site. Soaking the H72A TmPurL mutant crystals with FGAR, ADP, and $MgCl_2$ resulted in a structure containing $(Mg^{2+})_3$ -ADP. While the number of bound magnesium ions varies between complexes, one ion is observed in the same binding site for all structures

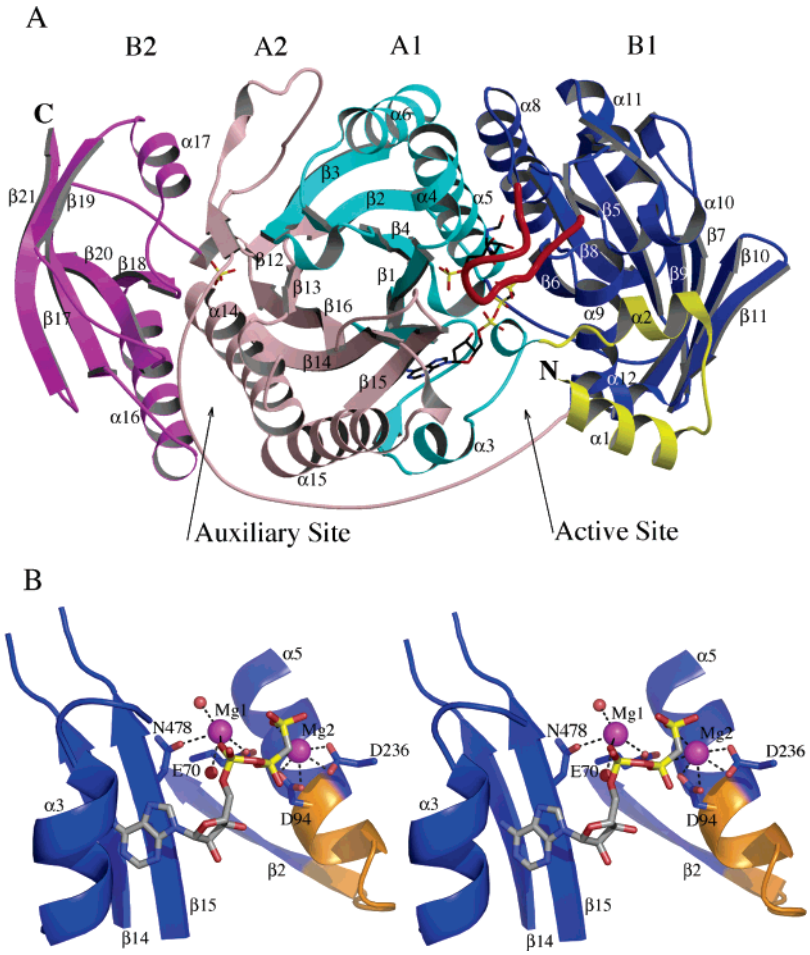


FIGURE 2: (A) Overall structure of the TmPurL−AMPPCP−FGAR ternary complex. TmPurL can be divided into four major subdomains: A1 (colored cyan), B1 (colored blue), A2 (colored pink), and B2 (colored magenta). Helices colored yellow are equivalent of the linker domain in StPurL (*10*). The loop colored red is disordered in the previously reported structures and becomes ordered upon FGAR binding. Shown in ball-and-stick representation are the AMPPCP and FGAR molecules bound in the active site and a phosphate ion bound in the auxiliary site. (B) Stereoview that zooms in on the bound nucleotide analogue (colored gray). The signature binding motif, $DX_4GAXP$, is highlighted in orange. Magenta spheres represent magnesium ions, and red spheres represent water molecules. Residues shown in ball-and-stick format are magnesium ligands.

and appears most relevant for nucleotide binding (see below).

As shown in Figure 2A, the active site is located in a cleft formed by the A1, A2, and B1 subdomains. In the TmPurL−FGAR−AMPPCP ternary complex, the substrate analogue (AMPPCP) is bound in the active site. The adenine base of the nucleotide is sandwiched between two parallel strands, $\beta$14 and $\beta$15, of subdomain A2 on one side and helix α3 of subdomain A1 on the other side (Figure 2B). Residues Tyr35, Ile42, Leu45, and Val474 make up the hydrophobic pocket for adenine binding (Figure 3). The N6 atom of the adenine base donates a hydrogen bond to the side chain of Asn442, while N1 accepts a hydrogen bond from the same residue. Unlike most ATP binding motifs, which usually utilize acidic residues to form hydrogen bonds with the 2′- and 3′-hydroxyl groups of the ribose moiety, no interactions are observed between the ribose of AMPPCP and PurL. A highly conserved glutamate, Glu51, is located within hydrogen bonding distance of the ribose; however, the side chain of this residue is disordered, and its conformation could not be determined. The phosphate tail of AMPPCP is bound perpendicularly to a strand−loop−helix motif, composed of $\beta$6 and α9, of subdomain A2 via two magnesium ions, termed Mg1 and Mg2. Mg1 is coordinated by the α-phosphate of the analogue, Asn478, Glu70, and two water molecules. Mg2 is ligated by the $\beta$- and $\gamma$-phosphates of AMPPCP, Asp236, and Asp94 (Figure 3). All of the residues that serve as ligands to the magnesium ions are highly conserved among smPurLs and lgPurLs. While the coordination and positioning of Mg1 vary between complexes of different nucleotides, Mg2 binding is consistent for all structures.

The nucleotides from the other three complexes bind in the same location as and with an orientation similar to that of the AMPPCP molecule in the PurL−FGAR−AMPPCP ternary complex. The adenine ring utilizes the same hydrophobic contacts and hydrogen bonds in all four complexes. With the exception of the $\gamma$-phosphate, the overall interactions in phosphate tail binding are similar in all structures. Residues Tyr35 and Asn478, strictly conserved within PurLs, and magnesium ions are involved in the binding of the nucleotide phosphate groups. Glu70, Asp94, and Asp236, conserved throughout the PurM superfamily, serve as magnesium ligands. The Mg2 binding site, which utilizes Asp94 and Asp236 as ligands and consistently appears in all complexes, is likely to be conserved in PurLs. Moreover, Asp94 is part of the signature $DX_4GAXP$ motif, suggesting that Mg2 binding is conserved among PurM superfamily members.

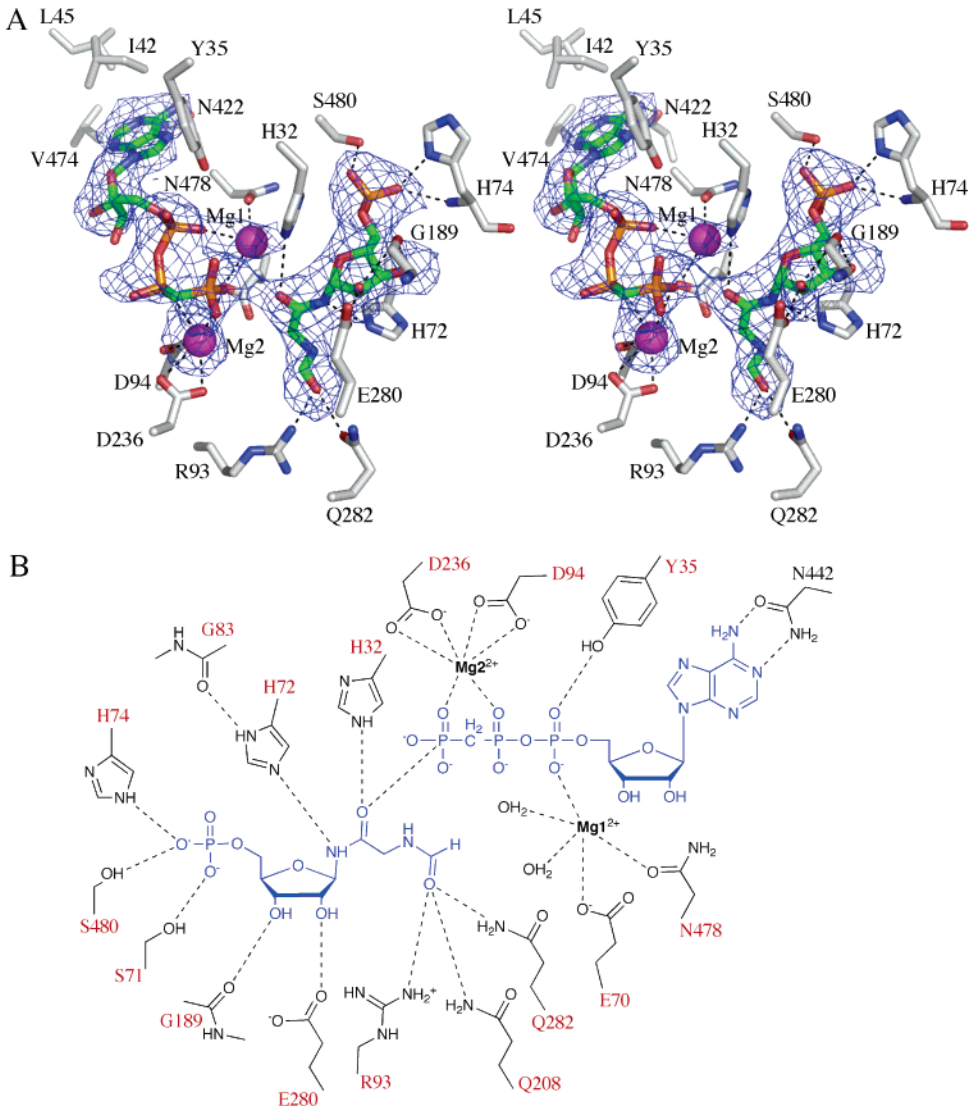


FIGURE 3: Active site of TmPurL. (A) Stereoview of the active site of the TmPurL−AMPPCP−FGAR ternary complex. FGAR and AMPPCP and residues that come in direct contact with the substrates are depicted using ball-and-stick representation. Magenta spheres represent magnesium ions. Hydrogen bonds and metal coordination bonds are depicted with dashed lines. $F_o - F_c$ density for the ligands and magnesium ions with a contour level of 1.5$\sigma$ is colored blue. (B) ChemDraw representation of the active site shown in panel A. Residues labeled in red are highly conserved among smPurLs and lgPurLs. D94 is the aspartate of the signature binding motif, $DX_4GAXP$.

In both the ATP and AMPPCP complexed structures, the $\gamma$-phosphate of the nucleotide points into the active site, but with different orientations. In the AMPPCP structure, the angle defined by the C and O atoms of the C6 carbonyl group of FGAR and the phosphorus atom of the $\gamma$-phosphate is approximately 160°. The C6 carbonyl oxygen atom is located 3.9 Å from the phosphorus atom and 3.5 Å from the closest phosphate oxygen atom. The $\gamma$-phosphate in the ATP complex was modeled with 50% occupancy pointing both into and away from the active site and FGAR binding location (Figure 4A). The high flexibility of the phosphate tail in the absence of the second substrate is a likely reason for the observed variations. This flexibility also results in greater thermal motion of magnesium ion Mg2, which has a *B* factor of 50, rather than <20, as observed for magnesiums in the other complexes.

A different conformation of a flexible loop that consists of residues 48−55 and caps the nucleotide from the solvent is observed between the various complexes (Figure 4A). In the H72A mutant TmPurL−AMPPCP structure, this loop is completely disordered, while in the other structures, the Cα backbone was clear but is observed in two conformations. In the ATP-bound complex, the orientation of this loop is ~180° opposite from that in the ADP binary and FGAR−AMPPCP ternary complexes. In the latter complexes, the loop is brought closer to the nucleotide binding site compared to the ATP complex with a root-mean-square deviation (rmsd) of 10 Å determined using PROFIT (*29*). In all complexes, the interactions between the loop and ATP, as well as the rest of the protein, are unclear due to poor side chain density. However, the loop is positioned to partially shield the nucleotide from the solvent upon complex formation.

*Auxiliary ATP Binding Site.* Soaking the wt TmPurL crystal with ATP resulted in an ATP molecule bound in the auxiliary binding site as well as the active site. This site is related to the active site by 2-fold pseudosymmetry (Figure 2A). The auxiliary ATP is located in a cleft between the central $\beta$-barrel, subdomains A1 and A2, and the N-terminal sheet and helices of subdomain B2. The hydrophobic pocket of the adenine ring consists of Leu109, Ile119, Leu138, Ala366, and Phe370 (Figure 5). The N6 atom of the adenine

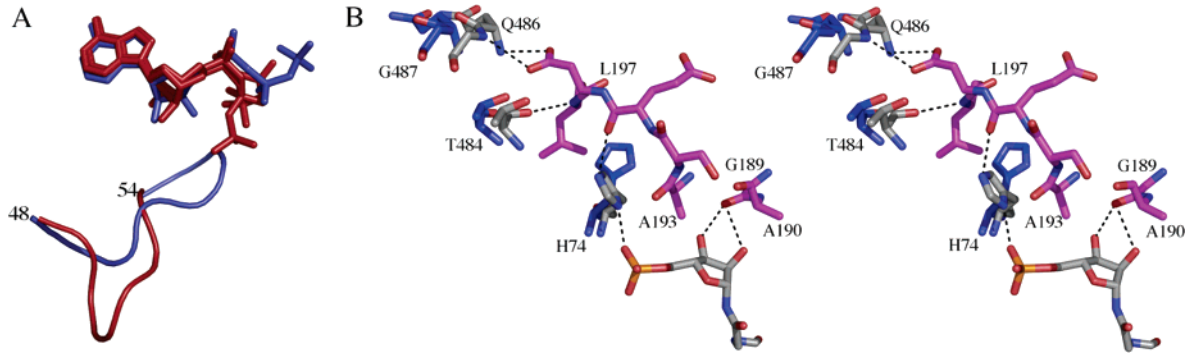


FIGURE 4: Conformation changes in the active site. (A) Superposition of AMPPCP from the ternary complex (blue) with the ATP molecules from the ATP complex (red) showing the flexibility of the phosphate tail. The loop capping the nucleotide from the bottom is shown as a ribbon illustrating the variation in conformation. (B) Stereoview of a superposition of the FGAR-bound vs unbound complexes. Colored blue is the uncomplexed enzyme, and colored gray and magenta is the complexed enzyme. Magenta indicates the part of the large loop that becomes ordered upon FGAR binding and gray the residues that shift upon FGAR binding.

base donates hydrogen bonds to Asp107 and Glu137, while the N1 atom accepts a hydrogen bond from Asp107, assuming that Asp107 is protonated in a buried environment. The 2′-hydroxyl group of the ribose ring interacts with the backbone of Gly136. The 3′-hydroxyl group is bound by the backbone carbonyl of Gly388 and the amide nitrogen of Gly386. All three phosphates of the ATP molecule are ligated by a magnesium ion. Additionally, the $\beta$-phosphate hydrogen bonds to His556, and $\gamma$-phosphate interacts with Arg139, His405, Lys429, Ser548, and Ser549. Residues Gly136, Glu137, and Gly386 are highly conserved among smPurLs (Figure 5B).

When the auxiliary ATP binds, some conformational changes in the enzyme are observed compared to the unbound structures. The most dramatic movement with a rmsd of 5 Å is that of a strand consisting of residues 363−373 toward the ATP molecule, bringing some of the hydrophobic residues such as Ala366, Val369, and Phe370 closer to the adenine moiety of ATP. Another notable change is the flipping of the backbone carbonyl of Pro385, which is part of a turn utilized in binding the ribose of the ATP molecule. In the absence of the auxiliary ATP, this carbonyl group hydrogen bonds to the backbone amide of Gly388. When ATP binds, Gly388 interacts with the 3′-hydroxyl group of the ribose moiety of the nucleotide; in turn, the carbonyl of Pro385 flips to avoid a close contact with ATP, and the amide nitrogen of Gly386 forms a hydrogen bond with the 2′-hydoxyl group of the ribose (Figure 5C). Residues 373−378 were excluded from the model of the ATP complex due to the lack of density; this region is present in the other structures.

Even though phosphate was absent from the purification buffers or the crystallization conditions of TmPurL, a strong phosphate density was found in the ternary AMPPCP−FGAR and binary AMPPCP structures. The phosphate ion is located at the $\gamma$-phosphate position of the auxiliary ATP (Figure 5B). It accepts hydrogen bonds from Arg139, Ser548, Ser549, and Lys429.

A comparison of the two symmetry-related ATP binding sites reveals sufficient differences to suggest that the auxiliary site is not catalytic. The active site lacks positively charged residues utilized in ATP binding by the auxiliary site. The hydrogen bonding network between the enzyme and the ribose, as well as the unusual magnesium binding utilizing all three phosphates of the ATP, is also absent in the active site of TmPurL. Mutagenesis data (described below) further confirm that the enzyme contains only one active site.

*FGAR Binding and the Associated Conformational Change.* The structure of the TmPurL ternary complex with FGAR and AMPPCP and the structure of the TmPurL−FGAR binary complex show a FGAR molecule bound in the active site of the enzyme (Figure 3). The orientation of the FGAR molecule in both complexes is identical. It is held in place through hydrogen bonding to residues that are highly conserved among smPurLs and lgPurls; these residues include His32, Ser71, His72, Asn73, His74, Arg93, Glu280, Gln282, and Ser480. The proximity of His32 and His72 to the site of amidine formation suggests that these residues play roles in catalysis. As discussed subsequently, these residues were targeted for mutagenesis. The phosphate moiety of FGAR is ligated by Ser71, Asn73, His74, and Ser480. The 2′-hydroxyl group of the ribose moiety donates a hydrogen bond to Glu280, while the 3′-hydroxyl group donates a hydrogen bond to the backbone carbonyl of Gly189. This ribose 5′-phosphate binding site is distinct from that found in other purine biosynthetic enzymes (*5*). The formyl group is bound by Arg93, Gln208, and Gln282 (Figure 3B).

A loop of 22 residues (186−207) that is disordered in both the deposited TmPurL and StPurL structures is ordered in both FGAR-bound structures (Figures 2A and 4B). This loop comes directly in contact with the substrate via residue Gly189 that accepts hydrogen bonds from the 2′- and 3′-hydroxy groups of the FGAR ribose moiety. Gly189 in turn donates a hydrogen bond to Ala193 within the loop (Figure 4B). While the backbone of His74 interacts with the phosphate moiety of FGAR, the side chain hydrogen bonds to the main chain of Glu195, also within the loop. Ala190 and Ser194 form a hydrogen-bonded pair. These interactions involving residues 188−195 allow formation of a small α-helical segment, α7. The rest of the region (residues 196−205) comes in contact with a loop of residues 482−489 in subdomain A2. This loop shifts by approximately 2.5 Å compared to the apo structure to satisfy hydrogen bond interactions with the previously disordered region. The side chain of Asp196 donates a hydrogen bond to the main chain of Thr484 and in turn accepts bonding from Gln486 and Gly487. Residues Leu197 and Thr484 also make a hydrogen

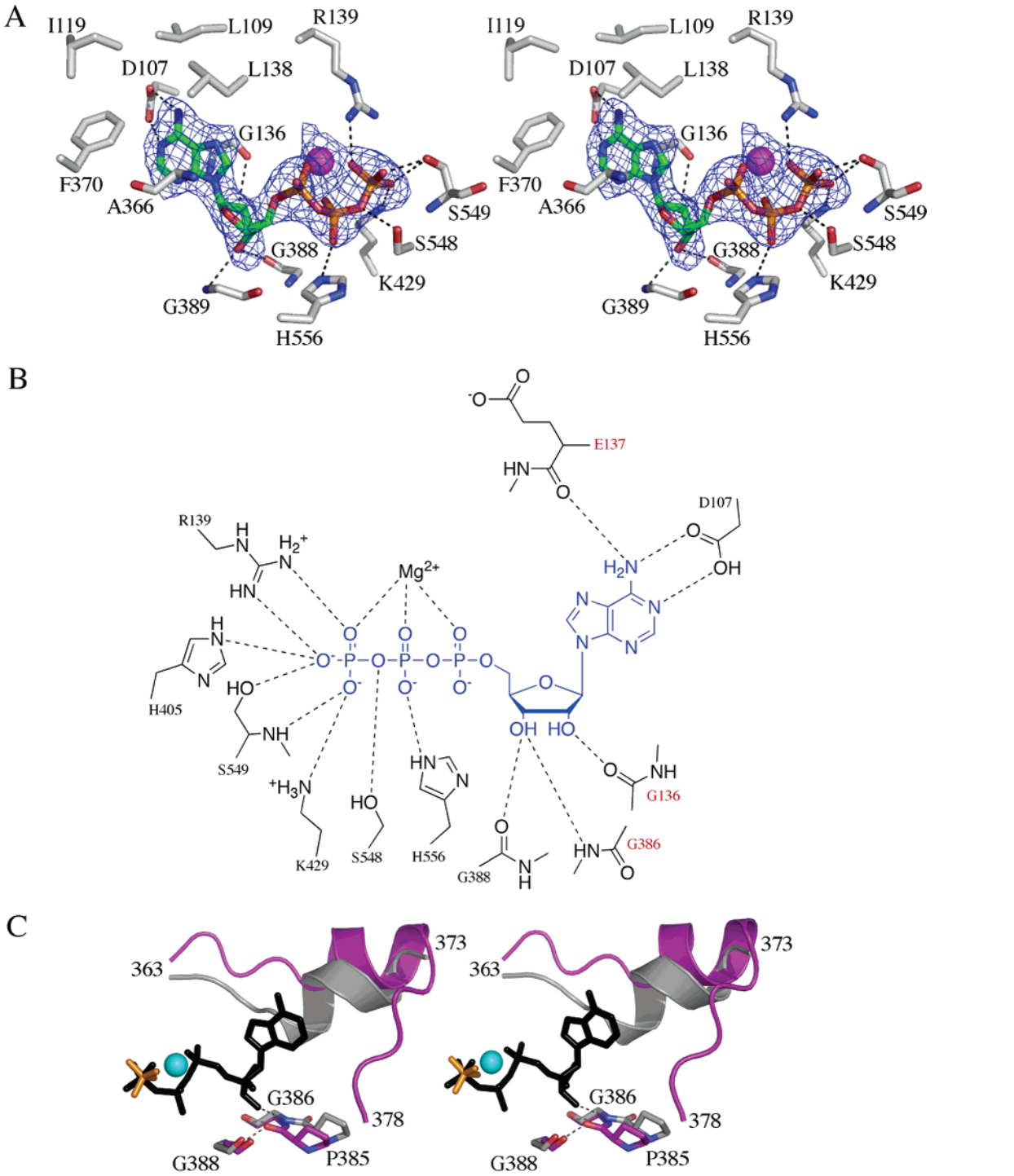


FIGURE 5: Auxiliary site of TmPurL. (A) Stereoview of the auxiliary site of the TmPurL−ATP ternary complex depicting, in ball-and-stick representation, direct interactions of the auxiliary ATP molecule with the residues of the protein. A magenta sphere represents a magnesium ion. Hydrogen bonds are depicted with dashed lines; $F_o - F_c$ density contoured at 2.5$\sigma$ is colored blue. (B) ChemDraw representation of the auxiliary site shown in panel A. Residues labeled in red are highly conserved among smPurLs. (C) Stereoview of the conformational changes associated with auxiliary ATP binding. ATP-bound TmPurL is colored gray, and the unbound form is colored magenta. The ATP molecule is colored black using ball-and-stick representation, and the magnesium ion is colored cyan; the phosphate ion present in the unbound structure is colored orange.

bonding pair. The ordering of the loop completely shields the FGAR molecule from the solvent and is likely to protect intermediates from hydrolysis.

*Activity of wt TmPurL*. Given that we have not yet reconstituted a *T. maritima* FGAR-AT complex from smPurL, PurQ, and PurS, we chose to assay smPurL activity by monitoring $NH_4Cl$-dependent FGAM synthesis. We have previously shown that in *B. subtilis* smPurL FGAM formation can be monitored by coupling the reaction to PurM or ADP formation can be monitored by coupling the reaction to PK/LDH (*13*). Intriguingly, the PK/LDH assay could not be used to monitor Gln-dependent product formation with the BsPurLSQ complex due to the appearance of long lag phases in the kinetics that were not present when BsPurL was assayed in the absence of PurS and PurQ with $NH_4Cl$ as the nitrogen source (*13*). This eventually led to the

Table 3: Kinetic Parameters for TmPurL

| | $K_m$ (mM) | $k_{cat}$ ($s^{-1}$)[a] |
|---|---|---|
| wt enzyme | | |
| FGAR | 1.05 +/− 0.06 | 0.40 +/− 0.01 |
| ATP | 0.26 +/− 0.04 | 0.41 +/− 0.02 |
| $NH_4Cl$ | 158 +/− 10[b] | 0.39 +/− 0.01 |
| H32A mutant | ND[c] | <0.0001[d] |
| H32Q mutant | ND[c] | <0.0001 |
| H72A mutant | | |
| FGAR[e] | ~38 mM | ~0.020 |
| H72Q mutant | ND[c] | 0.0019 +/− 0.0003[f] |

[a] Activity calculated from $V_{max}$ as determined using eq 1. [b] This corresponds to a $K_m$ of 5.7 mM for $NH_3$. [c] Not determined. [d] No activity could be detected above the lower limit of detection for the Bratton−Marshall assay. [e] The H72A mutant could not be saturated with FGAR, and severe substrate inhibition was observed above 16 mM, making it difficult to calculate an accurate $K_m$. In addition, $K_m$ values for ATP and $NH_4Cl$ could not be accurately determined due to the inability to saturate with FGAR, the high background ATPase, and the poor sensitivity of the PK/LDH assay. [f] Activity determined at 8 mM FGAR in the presence of 750 mM $NH_4Cl$ and 10 mM ATP. An identical activity was determined at 4 mM FGAR, suggesting the enzyme was saturated; however, the low activity prevented further analysis.

realization that ADP was acting as a necessary structural cofactor for assembly of the FGAR-AT complex (*13*).

At 37 °C and pH 8.0, we were readily able to demonstrate TmPurL FGAM synthetase activity (~0.34 unit/mg, Table 3). A contaminating ATPase (~7% of wt FGAM synthesis) was present in all enzyme preparations (including the H32 and H72 mutants described below) and was subtracted from initial velocity measurements. As with the *B. subtilis* enzyme, the $NH_4Cl$-dependent activity is not ADP-dependent, since inclusion of PEP and PK in the assay buffer had no effect on the observed activities. Assays were attempted at higher temperatures to replicate the physiological conditions for the thermophilic enzyme; however, precipitation was observed at ≥50 °C, and these experiments were not pursued further. It is possible that the enzyme is only heat-stable as the assembled FGAR-AT complex.

A kinetic analysis of the enzyme revealed several interesting features (Table 3). First, the $k_{cat}$ values for both the ATPase and FGAM synthetase activities are very close (0.40 and 0.41 $s^{-1}$), indicating ATP hydrolysis is coupled to FGAM formation. Second, it is interesting to note that the enzyme can be readily saturated with $NH_4Cl$ ($K_m$ = 158 mM). Assuming that the enzyme uses $NH_3$ as its actual substrate, this corresponds to a $K_m$ of 5.7 mM at pH 8.0, indicating that the enzyme displays binding characteristics similar to those of BsPurL ($K_m$ = 3.5 mM) (*13*). Finally, given that these assays are conducted under nonphysiological temperature and salt conditions in the absence of the PurS and PurQ subunits and with $NH_4Cl$ rather than the natural substrate, glutamine, we were particularly surprised by the very high activity displayed by this enzyme ($k_{cat}$ ~ 0.4 $s^{-1}$). This turnover is nearly 10-fold higher than any other reported $NH_4$-Cl-dependent activity for a FGAR-AT (*9*, *13*, *30*). After the *T. maritima* FGAR-AT complex has been assembled in vitro, it will be interesting to determine what similarities are shared with the *B. subtilis* FGAR-AT complex.

*Binding of ADP and ATP by TmPurL*. In the case of StPurL, the ADP cofactor occupying the auxiliary site is bound so tightly that it copurifies with the enzyme and can be removed only by protein denaturation (*10*). ADP binding in the *B. subtilis* smPurL appears to be slightly weaker, although rapid protein aggregation above 4 °C in the absence of ADP has made its binding difficult to study (A. Hoskins and J. Stubbe, unpublished results). The binding of ATP in the auxiliary site in one of our crystal structures raised the possibility that ATP, rather than ADP, acts as a tight-binding structural component with TmPurL.

Table 4: Binding of Nucleotide to TmPurL

| | incubation time (min) | incubation temperature (°C) | pH | nuleotide:protein molar ratio |
|---|---|---|---|---|
| wt enzyme | | | | |
| 3 mM ADP | 5 | 37 | 8.0 | 0.042 +/− 0.024:1 |
| 3 mM ATP | 5 | 37 | 8.0 | 0.74 +/− 0.07:1 |
| 1 mM ATP | 30 | 25 | 8.0 | 0.66 + /−0.09:1 |
| 1 mM ATP | 30 | 25 | 7.0 | 0.70 +/− 0.05:1 |
| H32A | | | | |
| 3 mM ATP | 5 | 37 | 8.0 | 0.74 +/− 0.03:1 |
| H72A | | | | |
| 3 mM ATP | 5 | 37 | 8.0 | 0.45 +/− 0.01:1 |

To address this question, binding of [$^{14}$C]ADP or ATP to TmPurL was monitored in solution by incubation of the nucleotide and enzyme at 37 °C and pH 8.0, followed by separation of the protein and unbound nucleotide at room temperature (Figure 3 of the Supporting Information). Experiments were also carried out to mimic crystallization conditions (25 °C and pH 7.0). The results are summarized in Table 4. They indicate that while only a small amount of ADP can be isolated with the enzyme (0.04 equiv), the enzyme readily forms an isolatable complex with ATP (0.7 equiv). The calculated stoichiometry is based upon an extinction coefficient of TmPurL [from ProtParam (www.expasy.ch)].

The ATP binding data are reminiscent of observations made by both the Buchanan and Stubbe laboratories on the chicken liver FGAR-AT. Buchanan and colleagues noted many years ago that this enzyme has the unusual property of being able to form a tight, isolatable complex with FGAR and ATP (0.7 ATP/enzyme ratio) in the absence of glutamine (*30*, *31*). The ATP likely binds in the active site of chicken liver PurL, as the auxiliary site should contain ADP on the basis of sequence homology with StPurL. In contrast, *E. coli* lgPurL is unable to form an isolatable complex with ATP in the presence or absence of FGAR (*32*). Therefore, at least one, but not all, FGAR-AT enzymes can bind substrates tightly. We favor the idea that tight ATP binding in TmPurL is occurring in the auxiliary site and not the active site on the basis of the $K_m$ for ATP (260 $\mu$M); however, more work is necessary to rule out tight, active site ATP binding for TmPurL.

*Activity of H32A(Q) and H72A(Q) TmPurL*. The crystal structures of TmPurL in the presence of substrates, substrate analogues, and products implicate the role of two conserved histidine residues in catalysis. To investigate this proposal further, four site-directed mutants of the enzyme were constructed and assayed using procedures developed for the wt enzyme. No FGAM synthetic activity was detected for either the H32A or H32Q mutant, indicating that the rate is less than 1/4000 of that of the wt enzyme. This result implicates His32 as playing an essential catalytic role.

The H72A mutant displayed 1/20 of the wt activity with a dramatically increased $K_m$ for FGAR (Table 3). In contrast, the H72Q mutant displayed 1/200 of the wt activity, and a

$K_m$ could not be determined due to the slow turnover. Results with the H72A and H72Q mutants indicate that this residue is not essential for catalysis but may function as a general base catalyst given its position adjacent to the FGAR amide and is important for FGAR binding.

An additional conclusion that can be drawn from the H32A(Q) and H72A(Q) mutants is that mutation of active site residues inactivates the enzyme despite leaving the auxiliary ATP-binding site intact. This indicates that despite having the capacity to bind the ATP substrate, the auxiliary site is not capable of $NH_4Cl$-dependent FGAM synthesis.

*Biophysical Characterization of wt and Mutant TmPurL.* Given the many problems we have encountered with protein aggregation with BsPurL (*13*), it was important to determine that the effects on activity observed with the *T. maritima* H32 and H72 mutant enzymes were due to the active site mutations rather than protein aggregation or unfolding. To address protein folding, CD spectroscopy and SV-AUC experiments were carried out.

As shown in Figure 4 of the Supporting Information, CD spectra of the wt and mutant enzymes are similar, indicating that the mutant enzymes are folded. Previous studies on Bs smPurL demonstrated aberrant behavior on gel filtration (*13*) but normal behavior on SV-AUC (*33*). Therefore, to look for aggregation on the TmPurL, we carried out SV-AUC experiments. The data (Figure 5 of the Supporting Information and Table 2) indicate that the predominant species in solution for both the wt and mutant enzymes is the smPurL monomer. Higher-molecular mass aggregates were observed for only the H72A mutant and correspond to ~26% of the total protein species. The CD and SV-AUC data indicate that the loss of activity observed with the H32 and H72 mutant enzymes is likely due to the absence of the histidine side chain rather than protein misfolding or aggregation.

*Active Site of the H72A Mutant.* Structural analysis of H72A PurL in comparison to the wt structure revealed that this mutation did not affect the active site globally. No dramatic changes in the position of the mutated residue and surrounding residues are observed. The mutation appeared to have no effect on the ATP binding site. However, it did affect binding of FGAR. All cocrystallization attempts with FGAR and the mutant under identical conditions that were successful with the wt protein were unsuccessful. Moreover, soaking FGAR into the native protein crystals completely destroyed them, while soaking of the mutant at equivalent concentrations resulted in no physical change in the crystals.

## DISCUSSION

*ATP-Binding Motif of the PurM Superfamily.* TmPurL is a member of the PurM superfamily of ATP-utilizing enzymes that contain the $DX_4GAXP$ motif identified through BLAST searches and multiple-sequence alignments. This superfamily is quite small with only five members having been identified to date (Figure 1). While structures of three of these enzymes, StPurL, *E. coli* PurM, and *A. aeolicus* ThiL, have been determined, all are in the unliganded form (*6*, *10*). TmPurL complexes reported here thus provide the first structural insight into this novel ATP-binding motif.

The nucleotide molecule binds in a large cleft formed by the core of the enzyme, subdomains A1 and A2, and the N-terminal subdomain, B1 (Figure 2A). It binds close to the surface, with the ribose and the phosphate tail being largely exposed to the solvent. The solvent accessibility of the nucleotide is distinct from the mode of ATP binding in the ATP grasp motif used by several enzymes in the purine pathway. In the ATP grasp superfamily, MgATP binding triggers a conformational change that results in inaccessibility of the entire ATP molecule, not just the $\gamma$-phosphate. In the PurM superfamily, the adenine moiety of the ATP is sandwiched between the N-terminal ends of two parallel $\beta$-strands, $\beta$14 and $\beta$15, in subdomain A2 on one side and helix $\alpha$3 of subdomain A1 on the other side (Figure 2). The $\alpha$-helix exhibits amphipathic character, with several positively charged residues pointing to the solvent, and hydrophobic residues lining the adenine moiety.

The phosphate tail is bound via two magnesium ions perpendicular to a strand−turn−helix motif, $\beta$6 and $\alpha$9, of subdomain A2. The stabilization of the binding of the tail, mediated entirely through the magnesium ions, is very different from that in the classical mononucleotide binding fold or the ATP grasp motif where the phosphates of the ATP are bound by conserved positively charged residues. The turn in this strand−turn−helix motif contains three sequential glycines and an alanine (G388, A389, G390, and G391) which allow for its tightness. The fingerprint sequence initially used to identify the PurM superfamily, $DX_4GAXP$, makes up a helix−turn−strand motif, $\alpha$5 and $\beta$2, of the active site pocket (Figure 2B). Asp94 of the fingerprint serves as a ligand to one of the magnesium ions, while the GAXP motif participates in the formation of the central $\beta$-barrel. A flexible loop of subdomain A1 caps the nucleotide from the bottom upon binding.

Remarkably, all of the secondary structural elements, the hydrophobic pocket containing the helix with a large number of basic residues, the glycine-rich turn used in phosphate tail binding, and the flexible loop capping the nucleotide, are also observed in the active sites of large StPurL, EcPurM, and AaThiL (Figure 6A). Asp94 of the fingerprint sequence in TmPurL structurally aligns with Asp318 in StPurL, Asp94 in EcPurM, and Asp71 in ThiL. Also, the other magnesium binding residues and the residues that make up the hydrophobic pocket for adenine are strongly conserved among the family members (Figure 6B). These observations confirm that the members of the PurM superfamily were identified correctly so far, in spite of the low degree of sequence similarity and the short fingerprint region.

*Comparison of PurL and PurM Active Sites.* While the secondary structure used for ATP binding in the active site of TmPurL is very similar to that in the active site of PurM, the FGAR/FGAM versus FGAM/AIR binding sites appear to be quite different. The PurM structure lacks the helix composed of residues 20−37 ($\alpha$2) that binds the formyl group of FGAR and contains a catalytically important residue, His32. Also, the large loop that undergoes a disorder−order transition upon FGAR binding in PurL (residues 180−200) is absent in PurM. Both of these structural elements are used to bury the substrate deeply in the active site pocket of PurL.

In the reported EcPurM structure, the N-termini of two monomers (residues 5−20) were found to partially cover the active site cleft, while the N-termini of the other two monomers in the crystallographic asu were disordered (*6*). Sequence alignments reveal that Tyr9, Gly13, Val14, Asp15,

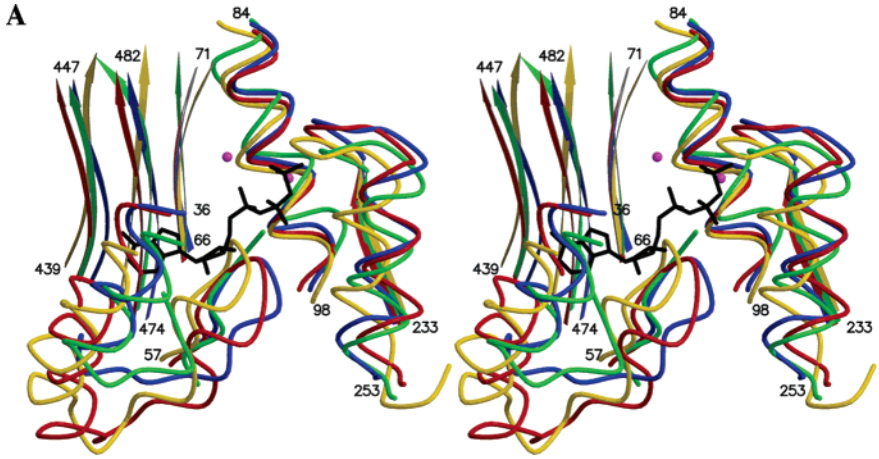


B

| | | | | | | | | | |
|---|---|---|---|---|---|---|---|---|---|
| *TmPurL* | 36 | SHTKKYIRR-LPK | 67 | FKIESH | 72 | | | | |
| *StPurL* | 220 | KIFN-LFKKMIKN | 291 | MKVETH | 296 | | | | |
| *EcPurM* | B21 | AL-VGRIKGVVKK | A62 | SGTDGV | A67 | | | | |
| *AaThiL* | A10 | GL-IDLIKKTLES | A40 | LTTDVL | A45 | | | | |
| *TmPurL* | 85 | ATGVGGIIRDVLAMGARP | 102 | 233 | GAQDLGAGGVLSATSELV | 250 | | | |
| *StPurL* | 309 | ATGSGGEIKDEGATGAKP | 326 | 499 | FIHDVGAGGLSNAMPELV | 516 | | | |
| *EcPurM* | A85 | IDLVAMCVNDLVVQGAEP | A102 | A244 | AIAHLTGGGFWENIPRVL | A261 | | | |
| *AaThiL* | A62 | WKAISVNVSDVIANGGLP | A79 | A204 | ASMDIS-DGLVADANKLA | A221 | | | |
| *TmPurL* | 440 | ITNCVNYG | 447 | 474 | VASGNASLY | 482 | | | |
| *StPurL* | 736 | LSANWMAA | 743 | 772 | IPVGKDSMS | 780 | | | |
| *EcPurM* | B105 | FLDYYATG | B112 | B137 | LVGGETAEM | B145 | | | |
| *AaThiL* | B82 | ALISLNLP | B89 | B115 | VVGGNISKS | B123 | | | |

FIGURE 6: (A) Stereoview of the nucleotide-binding pocket of the novel ATP-utilizing superfamily: superposition of TmPurL (blue), StPurL (red), EcPurM (yellow), and AaThiL (green). The black stick figure represents the AMPPCP molecule bound in the active site of TmPurL, and the magenta spheres are the magnesium ions. The numbering is of the TmPurL residues that make up the pocket. (B) Sequence alignment of the residues involved in ATP binding in the active site based on the structural superposition of TmPurL, StPurL, EcPurM, and AaThiL. Residues highlighted in red are highly conserved among the members of the novel ATP binding family, and residues highlighted in yellow are strongly conserved.

and Gly19 are all conserved among PurMs and could play important functional roles. On the basis of the structural superposition of TmPurL and EcPurM, the N-terminus of PurM could serve the same function as α2 (residues 20−37) of PurL and partially shield the active site. However, a conformational change moving the N-terminus closer to the active site would be necessary to accomplish this task.

The superposition of the PurM and PurL structures also reveals that in PurM a highly conserved helix α5 (residues 190−205) extends at an angle of approximate 90° away from the large flexible loop of PurL and away from the active site (Figure 7A). The area occupied by the base of this helix overlaps with that occupied by FGAR in PurL. PurM could undergo a different conformational change to bind its substrate: a reorientation of the helix−loop motif in the active site instead of an ordering of a similar motif as seen in PurL. This movement would allow for the extra room in the active site pocket needed to bind FGAM. It would also cover the substrate, thus providing a more stabilizing environment and preventing hydrolysis of the reacting intermediates.

In EcPurM, a sulfate molecule is bound in the active site in a position proposed to be the binding location for the 5′-phosphate of the FGAM molecule (*6*). The superposition of the PurM and PurL structures places the sulfate ion 6 Å from the 5′-phosphate of the FGAR molecule and 10 Å from the γ-phosphate of ATP. This observation suggests that FGAM will bind in a different orientation in PurM compared to PurL. Also, there are two histidine residues, His190 and His247, strictly conserved among PurMs, found in the active site of EcPurM (Figure 7B). The location and orientation of these histidine residues are different from those of the conserved His32 and His72 in TmPurL. This observation would also support different FGAM binding, if the histidine residues indeed play similar roles in the catalytic mechanisms of both enzymes.

Whether PurM undergoes a conformational change to accommodate its substrate, whether FGAM itself binds differently, or whether both occur cannot be deduced from the simple comparison of the available structures of the two enzymes. A crystal structure of PurM in complex with FGAM or AIR as well as careful modeling of the substrate in the active site would provide more information about the binding site. This would allow for further speculation about the relationship between the two enzymes and their reaction mechanisms.

*Implications for the Catalytic Mechanism*. Several mechanisms have been proposed for amidine formation (Figure 8) (*34*). One involves nucleophilic attack on the amide carbonyl by ammonia which forms the tetrahedral intermediate or transition state (td or ts 1, respectively) that is then phosphorylated by ATP (td or ts 2). This intermediate collapses to generate FGAM. The second involves ATP phosphorylation of the amide oxygen which forms an iminophosphate. This intermediate then interacts with ammonia to generate the same td or ts 2 as in the previous mechanism that then collapses to form product. Both mechanisms have enzymatic precedent: the former in

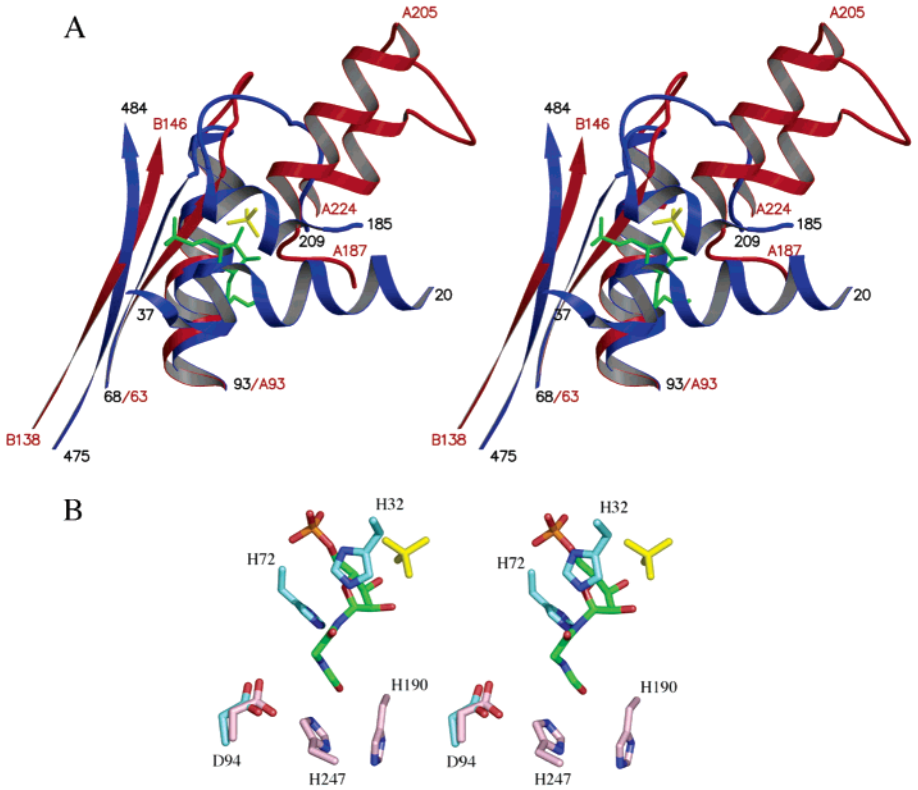


FIGURE 7: Comparison of the TmPurL and EcPurM active sites. (A) Stereoview of a superposition of TmPurL (blue) and EcPurM (red). FGAR bound in TmPurL is shown as a green ball-and-stick figure, and a sulfate ion bound in EcPurM is shown as a yellow ball-and-stick figure. Numbering in black is of TmPurL residues and in red is of EcPurM residues, with A and B labels used to distinguish the two monomers in the EcPurM dimer. (B) Close-up stereoview of the active site showing the conserved Asp94 from the $DX_4GAXP$ motif and the catalytic histidines. PurL is colored light blue with the FGAR molecule colored green, and PurM is colored pink with the sulfate ion colored yellow.

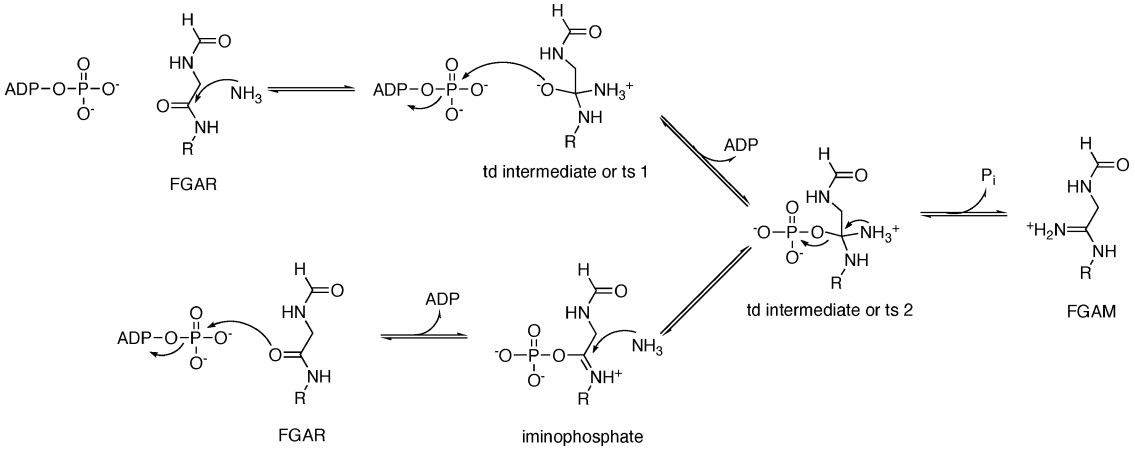


FIGURE 8: Two possible mechanisms for amidine formation originally proposed by Westheimer (*43*). R is ribose 5′-phosphate; td means tetrahedral and ts transition state.

glutamine synthetase catalyzed phosphorylation of the sulfoximine analogue of glutamine (*35*) and the latter in the CTP synthetase reaction (*36*). It should be noted that in glutamine synthetase, phosphorylation of the sulfoximine occurs on the nitrogen and not the oxygen of the inhibitor (*37*, *38*). An additional twist that can be accommodated within both mechanisms is the initial phosphorylation of the enzyme by ATP (*30*). Thus far, all efforts to provide evidence of intermediates in the lgPurL-catalyzed reaction have been unsuccessful (*30*, *32*).

The structure of the TmPurL−FGAR−$(Mg^{2+})_2$AMPCP complex, sequence alignments, and the resulting mutagenesis studies have demonstrated the importance of two histidines in catalysis. The location of His72, which is oriented by Gly83 in the active site (Figure 3B), suggests that it might function as a general base catalyst to remove a proton from $NH_4^+$ in mechanism 1 (Figure 8, top pathway) or to deprotonate the amide in mechanism 2 (Figure 8, bottom pathway). Rate decreases of 20−200-fold are not uncommon with mutations of general base catalysts in enzymes (*39*). It is likely that His72 also plays an important role in FGAR binding and in the orientation of the FGAR amide toward ATP. The role of His32 is more difficult to assess, although it is clearly essential for catalysis. The orientation of the $\gamma$-phosphate of ATP relative to this residue is key to defining its function. ATP analogues such as AMPPCP can have

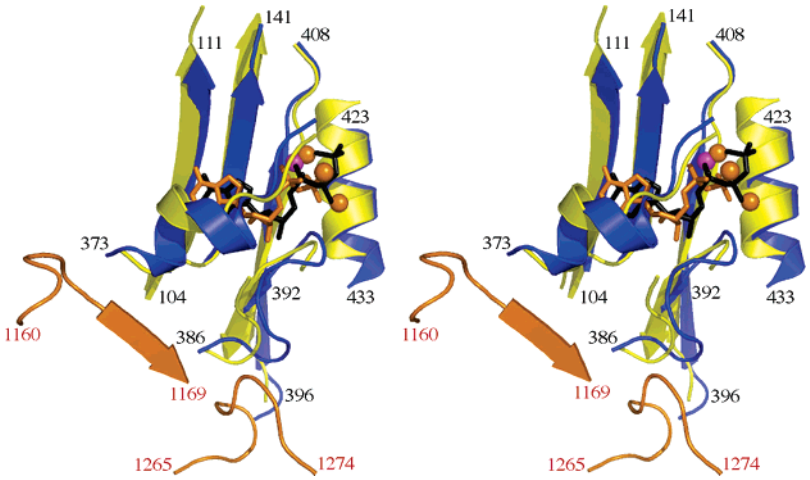


FIGURE 9: Comparison of the TmPurL and StPurL auxiliary sites. A stereoview of a superposition of the TmPurL−ATP complex (blue) and StPurL (yellow and orange). ATP bound in TmPurL is shown as a ball-and-stick figure colored black, and the magnesium ion is colored magenta; ADP bound in StPurL and the three associated magnesium ions are colored orange. StPurL is represented by two colors: yellow for the FGAM synthetase domain and orange for the glutaminase domain. The numbering in black is of TmPurL residues; the numbering in red is of the glutaminase domain of StPurL.

different metal coordination from ATP and consequently different phosphate orientations. With this caveat in mind, this residue could be involved in stabilization of the tetrahedral or iminophosphate intermediates. Alternatively, His32 could be involved in covalent catalysis. The exact role of each His and the identification of intermediates require further studies.

While the histidines are completely conserved in both lgPurLs and smPurLs, they are not conserved among other PurM superfamily members. Thus, it is unlikely that the common chemistry of the superfamily members involves an iminophosphate (Figure 1). Structure-based sequence alignments of family members and the ternary structure reveal it is only the ATP binding site that is conserved (Figure 6). If common chemistry is the unifying theme of these superfamily members, it likely involves only the role of the $\gamma$-phosphate in product formation. The phosphate binding sites are unusual because of the lack of positively charged amino acids. As first delineated from model studies, ATP hydrolysis likely involves a dissociative transition state (*40*), and this structure supports such a mechanism of phosphorylation in PurLs and, consequently, other superfamily members. This dissociative mechanism is in accord with early studies of Westheimer, who first postulated an iminophosphate intermediate generated by a "metaphosphate-like" transition state for this type of reaction (*34*). The detailed mechanism of ATP hydrolysis and phosphoryl transfer by PurM superfamily members also require further study.

*Role of the Auxiliary Binding Site*. Some of the members of the new ATP binding superfamily such as PurM, ThiL, and HypE are known to be dimers of approximately 35 kDa per monomer (*6*, *41*). However, TmPurL is a 66 kDa monomer that contains 2-fold pseudosymmetry also seen in the FGAM synthetase domain of large StPurL. In StPurL, an auxiliary site related to the active site by this 2-fold pseudosymmetry was discovered to contain an ADP molecule required for the structural integrity of the enzyme (*10*). Also it is known that small BsPurL requires MgADP for the formation of the PurLSQ complex, illustrating the regulatory role of this nucleotide (*13*).

On the basis of these results, TmPurL was thought to have an auxiliary ADP-binding site as well. Thus, it was a surprising discovery that this enzyme indeed binds ATP rather than ADP in its auxiliary site (Figure 5). Incubation of radiolabeled substrates followed by gel filtration allowed isolation of the complex of TmPurL with ATP but not ADP. This result further suggests that TmPurL is different from the *B. subtilis* enzyme, as BsPurL is known to bind ADP (*13*). However, the addition of TmPurQ and TmPurS could yield further surprises, and further work is needed on intact FGAR-AT complexes.

Structure-based sequence alignments strongly suggest that it is unlikely that the auxiliary site will catalyze FGAM synthesis. Futhermore, a comparison of the TmPurL active site and the auxiliary ATP site shows that there is insufficient space in the latter to accommodate a FGAR substrate molecule. The role of the auxiliary ATP, or possibly ADP in an intact TmPurLSQ complex, as a regulator required for formation of the PurLSQ complex is more probable. The superposition of StPurL and TmPurL shows a high degree of similarity in the location and binding orientation of the auxiliary ADP and ATP molecules, respectively (Figure 9). From this comparison, the most dramatic conformational changes upon ATP binding affect the secondary structural elements that should directly interact with PurQ (the glutaminase domain in lgPurLs). More specifically, the flexible loop−helix motif that is partially disordered upon ATP binding in TmPurL, residues 363−378 (residues 648−654 in StPurL), in superposition comes in contact with a large loop of the glutaminase domain, residues 1164−1170. Also, the large loop (residues 380−388 of TmPurL) involved in binding of the ATP molecule via Gly386 and Gly388 (Figure 5) superimposes onto residues 664−668 in StPurL that directly contact a loop, residues 1265−1275 of the glutaminase domain. Whether the conformational changes observed upon ATP binding are significant and whether they are the only change necessary for formation of the complex remain open questions.

In the AMPPCP, ADP, and FGAR complexes, a phosphate ion is bound in the auxiliary site at the position of the

γ-phosphate of ATP. Partial occupancy of the TmPurL auxiliary site by AMPPCP is observed when the concentration of the analogue is increased by a factor of 10 (data not shown). The tightly bound phosphate makes seven hydrogen bonds with nearby residues and is not displaced by the AMPPCP molecule as expected. The geometry of the methylene group and its electrostatics could prevent snug binding of the magnesium ion to all three phosphates; also, a hydrogen bond between the bridge oxygen and Ser548 would be missing in analogue binding. These small changes could altogether have a weakening effect on the binding of AMPPCP. A series of systematic high-resolution crystallographic experiments reported by Thoden et al. (*15*) confirm that nucleotide analogues, such as AMPPCP and AMPPNP, can exhibit binding behavior very different from that of the natural substrate (*15*).

*Evolutionary Implications. T. maritima* is a thermophilic eubacterium that appears to be deeply rooted in the eubacterial lineage and may be closely related to a bacterial progenitor that gave rise to the eubacterial, archaeal, and eukaryotic kingdoms (*42*). As such, the structure and properties of the auxiliary nucleotide binding site in TmPurL may shed light on early stages in the evolution of purine biosynthesis. PurL is clearly different from the other members of the PurM superfamily that function as homodimers and seems to have diverged early on. Following gene duplication and fusion from a PurM-like ancestor, subfunctionalization of the two active sites took place. The earliest smPurLs, possibly resembling TmPurL, may have retained ATP binding capacity in the auxiliary site and possibly exploited ATP binding to regulate formation of the PurLQS complex. Next, the regulation was modified to a structural ADP molecule that controls complex formation, as reported in *B. subtilis*. This change may have been accompanied by addition of structural elements to the smPurL. SmPurLs from Gram-positive and archaea bacteria are ~15 kDa larger than their counterpart in *T. maritima*. These regions may have evolved to fine-tune nucleotide binding by the auxiliary site. Finally, in Gram-negative bacteria and eukarya, complex formation was eliminated by fusing PurS and PurQ directly to smPurL to create lgPurLs. In this case, the ADP molecule became a purely structural feature of the active enzyme.

## CONCLUSION

A detailed description of the ATP-binding site in the PurM superfamily is presented for the first time. The nucleotide binds in a cleft formed by the core of the enzyme, subdomains A1 and A2, and a flanking subdomain, B1 (Figure 2A). The adenine moiety is sandwiched between two parallel β-strands, β14 and β15, and an α-helix, α3, while the phosphate tail is bound via magnesium ions perpendicular to a strand−turn−helix motif, β2−α5 (Figure 2B). These structural features are also observed in ThiL, PurM, and StPurL, which are other members of the superfamily (Figure 6A). Apart from the signature $DX_4GAXP$ sequence involved in the coordination of a magnesium ion, very little conservation of the primary sequence is observed between the superfamily members (Figure 6B). Lack of positively charged residues in the ATP-binding site appears to be characteristic of the PurM superfamily motif. Two histidine residues, His32 and His72, were found to be important for catalysis of PurL. On the basis of the available evidence, a dissociative mechanism for ATP hydrolysis is favored; however, neither of the two possible mechanisms (Figure 8) can be ruled out definitively. The chemical diversity of the second substrate in the PurM superfamily suggests that the unifying feature of this superfamily is the chemistry of the γ-phosphate transfer of the ATP molecule (Figure 1). An auxiliary site of TmPurL, structurally equivalent to the auxiliary ADP binding site of StPurL, was found to bind an ATP molecule and could play a regulatory role in formation of the PurLSQ complex (Figure 9).

## ACKNOWLEDGMENT

We thank Leslie Kinsland for assistance in the preparation of the manuscript. We thank the NE-CAT staff at beamline 8-BM and SER-CAT staff at Sector 22 of the Advanced Photon Source for assistance with data collection. The Biophysical Instrumentation Facility for the Study of Complex Macromolecular Systems at MIT is gratefully acknowledged.

## SUPPORTING INFORMATION AVAILABLE

A table of primers used in TmPurL cloning and mutagenesis, a table summarizing the SV-AUC results, the Coomassie-stained gels for TmPurL and mutants, a graph of the distribution of species obtained after SEDFIT analysis of SV-AUC data for wild-type and mutant TmPurL, a topology diagram of TmPurL, circular dichroism spectra for wild-type and mutant TmPurL, and an elution profile of wild-type TmPurL after incubation with radioactive ATP. This material is available free of charge via the Internet at http://pubs.acs.org.

## REFERENCES

1. Melnick, I., and Buchanan, J. M. (1957) Biosynthesis of the purines. XIV. Conversion of (α-N-formyl) glycinamide ribotide to (α-N-formyl) glycinamidine ribotide: Purification and requirements of the enzyme system, *J. Biol. Chem. 225*, 157−62.
2. Schulz, G. E. (1992) Binding of nucleotides to proteins, *Curr. Opin. Struct. Biol. 2*, 61−2.
3. Galperin, M. Y., and Koonin, E. V. (1997) A diverse superfamily of enzymes with ATP-dependent carboxylate-amine/thiol ligase activity, *Protein Sci. 6*, 2639−43.
4. Levdikov, V. M., Barynin, V. V., Grebenko, A. I., Melik-Adamyan, W. R., Lamzin, V. S., and Wilson, K. S. (1998) The structure of SAICAR synthase: An enzyme in the *de novo* pathway of purine nucleotide biosynthesis, *Structure 6*, 363−76.
5. Kappock, T. J., Ealick, S. E., and Stubbe, J. (2000) Modular evolution of the purine biosynthetic pathway, *Curr. Opin. Chem. Biol. 4*, 567−72.
6. Li, C., Kappock, T. J., Stubbe, J., Weaver, T. M., and Ealick, S. E. (1999) X-ray crystal structure of aminoimidazole ribonucleotide synthetase (PurM), from the *Escherichia coli* purine biosynthetic pathway at 2.5 Å resolution, *Struct. Folding Des. 7*, 1155−66.
7. Reissmann, S., Hochleitner, E., Wang, H., Paschos, A., Lottspeich, F., Glass, R. S., and Bock, A. (2003) Taming of a poison: Biosynthesis of the NiFe-hydrogenase cyanide ligands, *Science 299*, 1067−70.
8. Buchanan, J. M. (1982) Covalent reaction of substrates and antimetabolites with formylglycinamide ribonucleotide amidotransferase, *Methods Enzymol. 87*, 76−84.
9. Schendel, F. J., Mueller, E., Stubbe, J., Shiau, A., and Smith, J. M. (1989) Formylglycinamide ribonucleotide synthetase from *Escherichia coli*: Cloning, sequencing, overproduction, isolation, and characterization, *Biochemistry 28*, 2459−71.
10. Anand, R., Hoskins, A. A., Stubbe, J., and Ealick, S. E. (2004) Domain organization of *Salmonella typhimurium* formylglycina-

mide ribonucleotide amidotransferase revealed by X-ray crystallography, *Biochemistry 43*, 10328−42.
11. Anand, R., Hoskins, A. A., Bennett, E. M., Sintchak, M. D., Stubbe, J., and Ealick, S. E. (2004) A model for the *Bacillus subtilis* formylglycinamide ribonucleotide amidotransferase multiprotein complex, *Biochemistry 43*, 10343−52.
12. Batra, R., Christendat, D., Edwards, A., Arrowsmith, C., and Tong, L. (2002) Crystal structure of MTH169, a crucial component of phosphoribosylformylglycinamidine synthetase, *Proteins 49*, 285−8.
13. Hoskins, A. A., Anand, R., Ealick, S. E., and Stubbe, J. (2004) The formylglycinamide ribonucleotide amidotransferase complex from *Bacillus subtilis*: Metabolite-mediated complex formation, *Biochemistry 43*, 10314−27.
14. Marolewski, A., Smith, J. M., and Benkovic, S. J. (1994) Cloning and characterization of a new purine biosynthetic enzyme: A non-folate glycinamide ribonucleotide transformylase from *E. coli*, *Biochemistry 33*, 2531−7.
15. Thoden, J. B., Firestine, S. M., Benkovic, S. J., and Holden, H. M. (2002) PurT-encoded glycinamide ribonucleotide transformylase. Accommodation of adenosine nucleotide analogs within the active site, *J. Biol. Chem. 277*, 23898−908.
16. Sambrook, J., Fritsch, E. F., and Maniatis, T. (1989) in *Molecular cloning: A laboratory manual*, Vol. 3, Cold Spring Harbor Laboratory Press, Plainview, NY.
17. Sambrook, J., Fritsch, G. F., and Maniatis, T. (1989) in *Molecular Cloning: A Laboratory Guide*, Cold Spring Harbor Laboratory Press, Plainview, NY.
18. Otwinowski, Z., and Minor, W. (1997) Processing of X-ray diffraction data collected in oscillation mode, *Methods Enzymol. 276*, 307−26.
19. Brünger, A. T., Adams, P. D., Clore, G. M., DeLano, W. L., Gros, P., Grosse-Kunstleve, R. W., Jiang, J. S., Kuszewski, J., Nilges, M., Pannu, N. S., Read, R. J., Rice, L. M., Simonson, T., and Warren, G. L. (1998) Crystallography & NMR system: A new software suite for macromolecular structure determination, *Acta Crystallogr. D54*, 905−21.
20. Collaborative Computational Project Number 4 (1994) The CCP-4 suite: programs for protein crystallography, *Acta. Crystallogr. D50*, 760−3.
21. Jones, T. A., Zou, J.-Y., Cowan, S. W., and Kjeldgaard, M. (1991) Improved methods for the building of protein models in electron density maps and the location of errors in these models, *Acta Crystallogr. A47*, 110−9.
22. Laue, T. M., Shah, B. D., Ridgeway, T. M., and Pelletier, S. L. (1992) *Analytical Ultracentrifugation in Biochemistry and Polymer Science*, Royal Society of Chemistry, Cambridge, U.K.
23. Schuck, P. (2000) Size-distribution analysis of macromolecules by sedimentation velocity ultracentrifugation and Lamm equation modeling, *Biophys. J. 78*, 1606−19.
24. Lowry, O. H., Rosebrough, N. J., Farr, A. L., and Randall, R. J. (1951) Protein measurement with the Folin phenol reagent, *J. Biol. Chem. 193*, 265−75.
25. Kraulis, P. J. (1991) MOLSCRIPT: A program to produce both detailed and schematic plots of protein structures, *J. Appl. Crystallogr. 24*, 946−50.
26. DeLano, W. L. (2002) *The PyMOL Molecular Graphics Systems*, DeLano Scientific, San Carlos, CA.
27. Merritt, E. A., and Bacon, D. J. (1997) Raster3D: Photorealistic Molecular Graphics, *Methods Enzymol. 277*, 505−24.
28. Laskowski, R. A., MacArthur, M. W., Moss, D. S., and Thornton, J. M. (1993) PROCHECK: A program to check the stereochemical quality of protein structures, *J. Appl. Crystallogr. 26*, 283−91.
29. Martin, A. C. (1998) *PROFIT*, SciTech Software, London.
30. Mizobuchi, K., Kenyon, G. L., and Buchanan, J. M. (1968) Biosynthesis of the purines. XXXI. Binding of formylglycinamide ribonucleotide and adenosine triphosphate to formylglycinamide ribonucleotide amidotransferase, *J. Biol. Chem. 243*, 4863−77.
31. Schendel, F. J., and Stubbe, J. (1986) Substrate specificity of formylglycinamidine synthetase, *Biochemistry 25*, 2256−64.
32. Mueller, E. J. (1994) in *Chemistry*, Massachusetts Institute of Technology, Cambridge, MA.
33. Hoskins, A. A. (2006) in *Chemistry*, Massachusetts Institute of Technology, Cambridge, MA.
34. Satterthwait, A. C., and Westheimer, F. H. (1980) Monomeric methyl metaphosphate: Reactions with carbonyl groups, *J. Am. Chem. Soc. 102*, 4464−72.
35. Weisbrod, R. E., and Meister, A. (1973) Studies on glutamine synthetase from *Escherichia coli*. Formation of pyrrolidone carboxylate and inhibition by methionine sulfoximine, *J. Biol. Chem. 248*, 3997−4002.
36. von der Saal, W., and Villafranca, J. J. (1985) Cytidine-5′-triphosphate synthetase catalyzes the phosphorylation of uridine 5′-triphosphate by adenosine 5′-triphosphate, *J. Am. Chem. Soc. 107*, 703−4.
37. Rowe, W. B., Ronzio, R. A., and Meister, A. (1969) Inhibition of glutamine synthetase by methionine sulfoximine. Studies on methionine sulfoximine phosphate, *Biochemistry 8*, 2674−80.
38. Krajewski, W. W., Jones, T. A., and Mowbray, S. L. (2005) Structure of *Mycobacterium tuberculosis* glutamine synthetase in complex with a transition-state mimic provides functional insights, *Proc. Natl. Acad. Sci. U.S.A. 102*, 10499−504.
39. Kirby, A. J. (1997) Efficiency of Protron Transfer Catalysis in Models and Enzymes, *Acc. Chem. Res. 30*, 290−6.
40. Admiraal, S. J., and Herschlag, D. (1995) Mapping the transition state for ATP hydrolysis: Implications for enzymatic catalysis, *Chem. Biol. 2*, 729−39.
41. Blokesch, M., Paschos, A., Theodoratou, E., Bauer, A., Hube, M., Huth, S., and Bock, A. (2002) Metal insertion into NiFe-hydrogenases, *Biochem. Soc. Trans. 30*, 674−80.
42. Nelson, K. E., Clayton, R. A., Gill, S. R., Gwinn, M. L., Dodson, R. J., Haft, D. H., Hickey, E. K., Peterson, J. D., Nelson, W. C., Ketchum, K. A., McDonald, L., Utterback, T. R., Malek, J. A., Linher, K. D., Garrett, M. M., Stewart, A. M., Cotton, M. D., Pratt, M. S., Phillips, C. A., Richardson, D., Heidelberg, J., Sutton, G. G., Fleischmann, R. D., Eisen, J. A., White, O., Salzberg, S. L., Smith, H. O., Venter, J. C., and Fraser, C. M. (1999) Evidence for lateral gene transfer between Archaea and bacteria from genome sequence of *Thermotoga maritima*, *Nature 399*, 323−9.
43. Westheimer, F. H. (1981) Monomeric metaphosphates, *Chem. Rev. 81*, 313−26.

BI061591U